Geol. Mag. **144** (*5*), *2007, pp. 867–882.* © *2007 Cambridge University Press*

doi:10.1017/S0016756807003524 First published online 29 May 2007 *Printed in the United Kingdom*

Early to Middle Miocene intra-continental basaltic volcanism in the northern part of the Arabian plate, SE Anatolia, Turkey: geochemistry and petrogenesis

MUSA ALPASLAN*

Mersin University, Department of Geology, 33343, Çiftlikköy-Mersin, Turkey

(*Received* 21 August 2006; *accepted* 13 November 2006)

Abstract – Continental basalts ranging in age from 16.5 to 19.08 Ma crop out throughout the northern part of the Arabian plate. The basalts have distinctive petrographic characteristics such as rounded and skeletal olivine phenocrysts with abundant melt inclusions, implying the mixing of two distinct magmas. All of the analysed basalts are tholeiitic in composition. The presence of quartz xenocrysts with clinopyroxene rims in some samples indicates that crustal assimilation was probably an important process during magma ascent to the surface, and low Mg number and high SiO_2 contents of the basalts clearly show that they have experienced fractional crystallization as well as crustal contamination. Variations of the major and trace elements versus MgO show that olivine + clinopyroxene + plagioclase were the main fractionating minerals. In terms of incompatible trace elements, the basalts have OIB-like signatures with a slight depletion at Nb–Ta on primitive-mantle-normalized diagrams. The basalts have slightly LREE enriched patterns with $La/Yb_N = 5.5$ to 6.7. La/Nb ratios are close to unity, suggesting the melts may have originated in the asthenospheric mantle. Partial melting modelling based on REE data imply that the melts were not produced from a single mantle source depth, which is either purely a spinel- or garnet-peridotite end member. The samples lie on a binary mixing line between low-degree melts (< 5 %) from garnet-peridotite and higher-degree melts (> 10 %) from spinel-peridotite sources on a plot of La/Yb v. Dy/Yb, requiring interaction of melts derived from both garnet- and spinel-peridotite fields. Melts originating from both sources were initially tapped by distinct magma chambers, which subsequently hybridized into a single flow. Hybridized magma ascended to the surface along Neogene strike-slip faults, which are linked to the Dead Sea Fault Zone.

Keywords: basaltic volcanism, SE Anatolia, partial melting, magma mixing, Arabian plate.

1. Introduction

Continental intra-plate basaltic volcanism, commonly referred to as continental flood basalts (CFB), is formed by rapid eruption of huge volumes of the basalts in discrete events of geologically short duration. Despite their volumetric significance, some uncertainties remain about their sources and processes of formation. Generation of the most primitive magmas has been explained either by a mantle plume raising the mantle temperature (Richards, Duncan & Courtillot, 1989; White & McKenzie, 1989; Campbell & Griffiths, 1990) or lithospheric extension inducing decompressional melting (Turcotte & Emerman, 1983; Anderson, 1994; King & Anderson, 1995, 1998). Continental intra-plate basalts display a relatively restricted major element composition, similar to that of evolved mid-ocean ridge basalts (MORB); they are enriched in light rare earth elements (LREE) and large-ion lithophile elements (LILE), but relatively depleted in high field-strength elements (HFSE) with respect to LILE and LREE, when normalized to primitive mantle compositions (Cox & Hawkesworth, 1985). These characteristics have been attributed to crustal assimilation (Ellam & Cox, 1989), enriched subcontinental mantle (Ellam & Cox, 1991), mixing between depleted and enriched mantle domains (Campbell & Griffiths, 1990), and combinations of melting of enriched mantle and crustal assimilation (Arndt & Christiansen, 1992).

Extensive volcanic activity developed mostly during Neogene to present times on the Arabian plate (Fig. 1a; Çapan, Vidal & Cantagrel, 1987; Giannerini *et al.* 1988; Garfunkel, 1989; Heimann & Ron, 1993; Ilani *et al.* 2001), post-dating the break-up of Africa and Arabia, and opening of the Red Sea. During Cenozoic times, the northward motion of the Arabian plate caused tectonic reorganization with more or less contemporaneous igneous activity (Giannerini *et al.* 1988; Rukieh *et al.* 2005). The main stages are: (a) the development of the Dead Sea Fault Zone (also known as the Levantine fault system), a sinistral strike-slip fault with a total length of about 1000 km and a total displacement about 105 km (e.g. Garfunkel, 1981; LePichon & Gaulier, 1988; Heimann & Ron, 1993; Sobolev *et al.* 2005); (b) northward subduction of Neotethys and a final collisional event, which is responsible for the

* E-mail: malpaslan@mersin.edu.tr

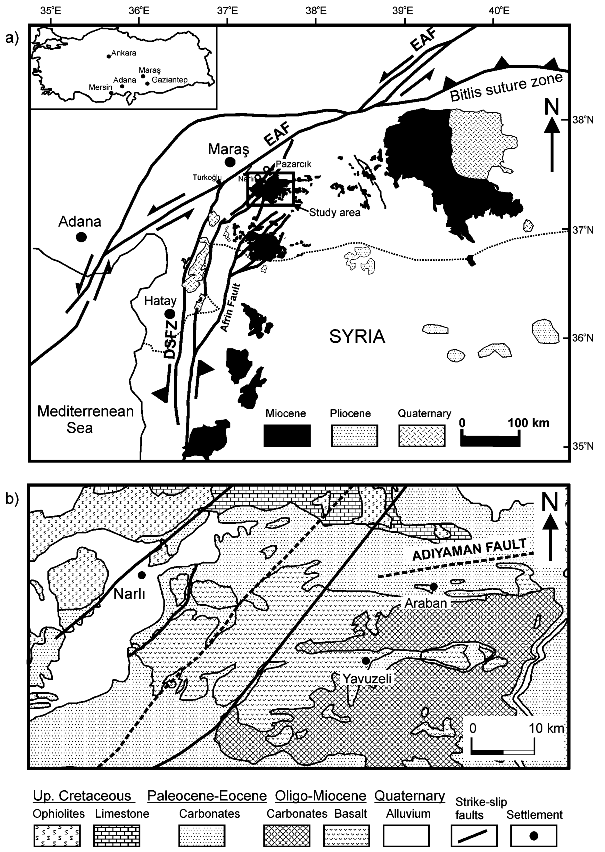

Figure 1. (a) Major tectonic structures of Turkey and location of the study area adopted from Yürür & Chorowicz (1998), Coşkun (2004), Westaway (2003, 2004), Rukieh *et al.* (2005) and Lustrino & Sharkov (in press) (DSFZ – Dead Sea Fault Zone). (b) Geological map of the study area (modified after MTA, 2002).

Bitlis–Zagros orogenic belt, between the Arabian and Eurasian plates (e.g. Perinçek, 1979; Şengör & Kidd, 1979; Yılmaz, 1993); (c) Neogene to present volcanic activity (e.g. A. Haksal, unpub. undergraduate thesis, Univ. Hamburg, 1981; Çapan, Vidal & Cantagrel, 1987; Ulu *et al.* 1991; Heimann & Ron, 1993; Polat, Kerrich & Casey, 1997; Sharkov *et al.* 1998; Alıcı *et al.* 2001; Bertrand *et al.* 2003; Shaw *et al.* 2003; Rukieh *et al.* 2005; Lustrino & Sharkov, 2006; Fig. 1a).

Most studies have focused on the Quaternary–present basaltic volcanism and tectonics in the northern part of the Dead Sea Fault Zone (e.g. Çapan, Vidal & Cantagrel, 1987; Polat, Kerrich & Casey, 1997; Yürür & Chorowicz, 1998; Arger, Mitchell & Westaway, 2000; Alıcı *et al.* 2001; Rojay, Heimann & Toprak, 2001; Tatar *et al.* 2004; Lustrino & Sharkov, 2006), but little attention has been paid to the Miocene basaltic volcanism in Southeast Anatolia (Ulu *et al.* 1991). Lustrino & Sharkov (2006) suggest that the basaltic volcanism occurs due to passive upwelling of the shallow asthenosphere, resulting from transtensional movements along the Dead Sea Fault Zone, during the development of the Dead Sea Fault Zone without influence from the nearby Afar mantle plume and passive decompression of the same sources during Miocene–Pliocene times. Quaternary basaltic volcanism north of Hatay has been related to extensional tectonics along the Dead Sea Fault Zone (Rojay, Heimann & Toprak, 2001; Alıcı *et al.* 2001).

In this paper, the whole range of geochemical data from the early–middle Miocene intra-continental basaltic volcanic rocks of Southeast Anatolia are reported for the first time. The objective of this study is to explain the magmatic processes and related geodynamics that are inferred from the petrographical and geochemical characteristics of the early–middle Miocene basaltic volcanism.

2. Geological framework

In the study area, lithological units vary from Upper Cretaceous to recent age (Fig. 1b). The Upper Cretaceous units are ophiolitic, and include serpentinized ultrabasic rocks, pillow lavas, limestone and shale (Fig. 1b), and were emplaced as a consequence of the convergence between Afro-Arabian and Eurasian plates. Tertiary units of Paleocene to Oligocene age mainly consist of shallow marine carbonates (Ulu *et al.* 1991). Since early–middle Miocene times, the northern part of the Arabian plate has been gradually uplifted and has evolved into a continental basin (Ulu *et al.* 1991). Basaltic volcanic rocks rest on the earlier units (Fig. 1b). Basaltic volcanism occurred in a time span between 16.5 and 19. 08 Ma based on K–Ar data (Arger, Mitchell & Westaway, 2000; Tatar *et al.* 2004). Four basaltic flows have been distinguished at the south of the Narlı district. Total thickness of the basaltic flows reaches up to 100 metres. The youngest unit in the study area is Quaternary alluvium (Fig. 1b).

3. Rock classification and petrography

Analysed samples fall in the basalt and basaltic andesite fields on the total alkali silica (TAS) plot (Fig. 2a), and show tholeiitic affinity on the AFM plot of Irvine & Baragar (1971; Fig. 2b). All basaltic samples, except one, are olivine-normative (Table 1). Samples are typically porphyritic with a holocrystalline groundmass and phenocrysts of euhedral to subhedral olivine. Phenocryst assemblages of both olivine + clinopyroxene and olivine + plagioclase have been seen in the highly porphyritic samples. The groundmass is typically intergranular to ophitic and consists predominantly of subhedral plagioclase laths, with clinopyroxene and minor oxides. Plagioclase phenocrysts commonly show zoning patterns (Fig. 3a). Some samples include quartz xenocrysts surrounded by pyroxene microlites (Fig. 3b). Phenocrysts of olivine, plagioclase and clinopyroxene occasionally occur as glomerophyric aggregates in the porphyrytic samples.

https://doi.org/10.1017/S0016756807003524 Published online by Cambridge University Press

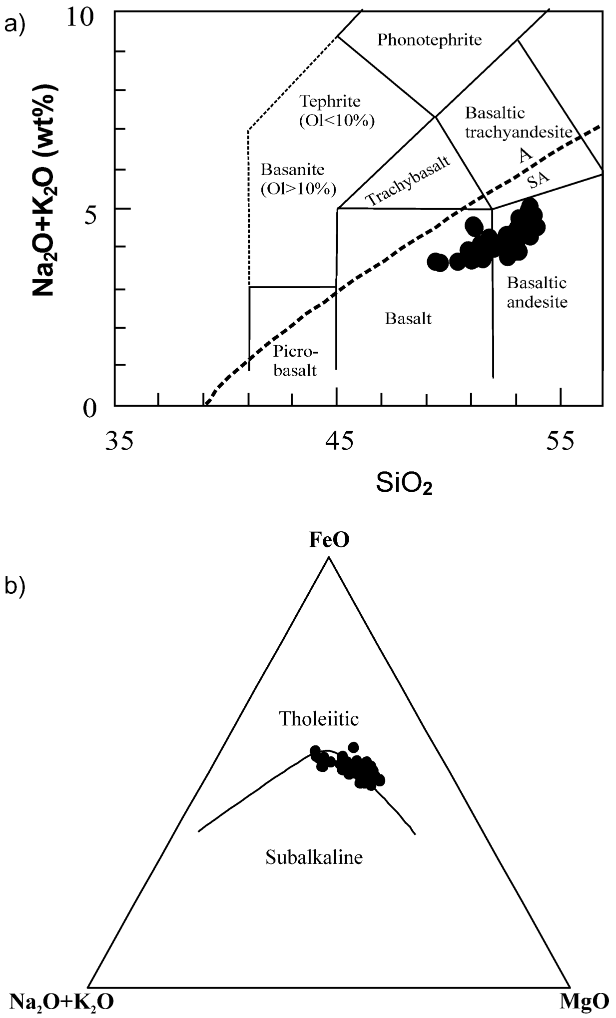

Figure 2. (a) Total alkali-silica nomenclature diagram of LeBas *et al.* (1986) for the early–middle Miocene volcanic rocks in southeastern Turkey. (b) AFM diagram of Irvine & Baragar (1971) for the studied volcanic rocks.

In some samples, glomerocrysts of clinopyoxene, which mainly are surrounded by olivine, have been observed (Fig. 3c).

The more primitive samples have predominantly small olivine phenocrysts (generally < 0.5 mm) within fine-grained groundmass, although evolved ones include olivine phenocrysts varying in size from < 0.3 to 2 mm. Phenocrysts of olivine commonly have iddingsite rims, although some of them are completely altered to iddingsite. Olivine occurs as euhedral to skeletal, embayed and rounded phenocrysts (Fig. 3d–f). Rounded to embayed olivine phenocrysts coexisting with smaller euhedral and skeletal phenocrysts of olivine possibly indicate the mixing of compositionally distinct magmas (Richter & Murata, 1966; Wright, 1973). Olivine phenocrysts contain abundant rounded and elongated melt inclusions (Fig. 3g). Some olivine phenocrysts are dendritic, implying rapid growth (Fig. 3h).

4. Geochemistry

Based on petrographical investigations, 44 representative samples were selected for major and trace element analyses. Major element analyses were determined by inductively coupled plasma-atomic emission spectrometry (ICP-AES). Trace and rare earth elements (REE) were determined by inductively coupled plasma-mass spectrometry (ICP-MS). All the analyses were carried out at the ACME Analytical Laboratories Ltd, Canada. Analytical precision is better than 0.5 % for major elements and 5 % for trace elements.

4.a. Major and trace elements

Chemical analyses and CIPW norms are listed in Table 1. Samples fall into the basalt and basaltic andesite fields below the dividing line for alkaline and subalkaline fields of Irvine & Baragar (1971) (Fig. 2a). The recovered samples contain between 8.74 % and 3.9 % MgO, implying some fractional crystallization, because none of the lavas represents a primary magma with Mg number greater than 0.68. Figure 4 shows the major elements plotted against MgO for early–middle Miocene volcanic rocks. The negative correlation between MgO and SiO_2 (Fig. 4) indicates variable degrees of fractional crystallization, involving initial removal of olivine in higher MgO. The increase of SiO_2 and decrease of Fe_2O_3t indicate that fractional crystallization of ferromagnesian minerals such as olivine and clinopyroxene may have played an important role in the evolution. TiO_2 does not correlate with MgO (Fig. 4), which implies that fractional crystallization of Ti-bearing opaques may not be very prominent in early–middle Miocene volcanic rocks. In the more magnesian rocks (MgO > 7 wt %), CaO decreases with decreasing MgO, suggesting that plagioclase fractionation occurs in this interval. However, the flat trend of CaO with decreasing MgO in the rocks with < 7 % MgO indicates that plagioclase fractionation is insignificant. Figure 5 presents some compatible and incompatible trace element variations plotted against MgO. As MgO decreases, there is a general decrease in the compatible trace elements such as Ni and Cr implying olivine and clinopyroxene fractionation. The increase of incompatible trace elements such as Rb, Zr, and Y and decrease of MgO suggest that crystal fractionation is one of the major magmatic processes in the evolution of the magma forming the early–middle Miocene volcanic rocks (Fig. 5). Nb/U ratios of more primitive samples resemble those of typical oceanic island basalts (Hoffmann *et al.* 1986), although those of evolved samples have values lower than OIB (Table 1), which possibly indicate crustal assimilation. Ce/Pb ratios vary from 26 to 95. High variability in the Ce/Pb values may have been caused by the mobility of Pb during secondary processes. A discrimination plot based on HFSE data

https://doi.org/10.1017/S0016756807003524 Published online by Cambridge University Press

https://doi.org/10.1017/S0016756807003524 Published online by Cambridge University Press

Table 1. Major and trace element compositions and normative mineralogies of the early to middle Miocene volcanic rocks (∗)

Sample no.	316	317	318	319	321	322	323	324	325	326	327	328	329	330	331	332
Longitude (E)	37° 16'27"	37° 16'33"	37° 16'32"	37° 16'32"	37° 16'29"	37° 16'29"	37° 16'29"	37° 16'29"	37° 16'29"	37° 16'29"	37° 16'32"	37° 16'33"	37° 16'31"	37° 16'31"	37° 16'35"	37° 16'36"
Latitude (N)	037° 12'10"	037° 12'12"	037° 12'11"	037° 12'11"	037° 12'27"	037° 12'27"	037° 12'27"	037° 12'27"	037° 12'27"	037° 12'27"	037° 12'30"	037° 12'30"	037° 12'26"	037° 12'26"	037° 12'23"	037° 12'23"
SiO_2	52.8	52.69	53.67	53.6	52.05	53.45	53.11	53.31	53.36	53.24	51.27	51.19	53.18	52.68	52.9	52.31
Al_2O_3	14.01	14.37	13.86	13.73	14.06	16.4	15.14	16.67	16.44	16.77	14.61	14.55	14.23	14.4	14.4	14.08
Fe_2O_3	11.2	11.03	10.71	10.86	11.78	10.18	10.86	9.9	10.08	9.86	11.94	11.95	11.14	11.29	11.33	11.02
MgO	7.29	7.24	6.35	6.67	6.61	3.68	5.36	4.03	4.22	4.35	5.85	6.37	6.61	6.5	6.4	7.23
CaO	7.87	7.98	7.9	7.74	8	8.36	8.15	8.43	8.47	8.42	7.76	7.77	8	8.07	7.98	8.55
Na_2O	3.15	3.13	3.2	3	3.08	3.64	3.22	3.6	3.44	3.56	3.51	3.44	3.13	3.29	3.18	3.13
K_2O	1	1.12	1.32	1.32	0.91	1.01	0.93	1.1	1.16	1.19	1.01	1.12	1.07	1.06	1.05	0.93
TiO_2	1.54	1.58	1.68	1.61	1.64	1.78	1.64	1.76	1.7	1.7	1.84	1.76	1.58	1.56	1.6	1.5
P_2O_5	0.22	0.21	0.27	0.24	0.23	0.23	0.2	0.23	0.22	0.23	0.26	0.28	0.22	0.21	0.24	0.22
MnO	0.13	0.13	0.12	0.13	0.13	0.11	0.11	0.1	0.11	0.11	0.13	0.14	0.12	0.13	0.12	0.12
Cr_2O_3	0.038	0.043	0.037	0.037	0.038	0.006	0.025	0.007	0.007	0.007	0.029	0.035	0.039	0.04	0.039	0.034
Total	99.97	99.95	99.94	99.96	99.95	99.96	99.96	99.94	99.81	99.95	99.94	99.94	99.95	99.96	99.96	99.95
LOI	0.7	0.4	0.8	1	1.4	1.1	1.2	0.8	0.6	0.5	1.7	1.3	0.6	0.7	0.7	0.8
Ni									47	42	213	247	196	197	183	191
Normative minerals																
Q	2.8	2.25	4.28	4.78	3.38	5.18	5.13	4.32	4.61	3.6	0	0	3.87	2.5	3.6	2.02
Or	5.92	6.63	7.82	7.82	5.39	5.98	5.51	6.51	6.87	7.04	5.98	6.63	6.34	6.28	6.22	5.51
Ab	26.65	26.48	27.07	25.38	26.06	30.8	27.24	30.46	29.11	30.12	29.7	29.11	26.48	27.84	26.91	26.48
An	21.15	21.87	19.57	20.11	21.87	25.45	24.13	26.1	26.01	26.29	21.14	20.97	21.63	21.41	21.93	21.64
Ne	0	0	0	0	0	0	0	0	0	0	0	0	0	0	0	0
Di	13.47	13.37	14.64	13.69	13.4	12.12	12.39	11.82	12.1	11.6	13.04	13.1	13.64	14.17	13.22	15.8
Hy	20.96	20.65	17.29	18.84	19.63	11.03	16.08	11.8	12.44	12.8	20.52	18.63	19.03	18.69	18.86	19.55
Ol	0	0	0	0	0	0	0	0	0	0	0.3	2.75	0	0	0	0
Mt	4.87	4.8	4.66	4.72	4.72	4.43	4.72	4.31	4.38	4.29	3.46	3.47	4.85	4.91	4.93	4.79
Il	2.92	3	3.19	3.06	3.11	3.38	3.11	3.34	3.23	3.23	3.49	3.34	3	2.96	3.04	2.85
Ap	0.52	0.5	0.64	0.57	0.55	0.55	0.47	0.55	0.52	0.55	0.62	0.66	0.52	0.5	0.57	0.52
Trace elements																
Ni	201	203	173	204	197	44	112	44								
Sc	17	17	16	16	17	16	18	16	16	16	16	16	17	17	17	17
Ba	178.7	170.5	182.2	160.5	139.4	222.6	207.1	217	219.6	213.4	176.6	198.3	183.2	189.4	187.9	171
Co	53	45	47.7	50.8	49.5	39.1	42.9	36.1	40.5	41.4	49.6	54.6	49.2	52.1	46.9	49.9
Cs	0.8	1	0.9	1	0.7	0.8	0.8	0.7	0.7	0.6	0.6	0.8	1.4	0.9	0.8	1
Ga	22.3	21.9	22.4	21.3	22.3	24.6	23.3	24	24.3	23.7	22.6	22.5	21.8	21.3	22.2	22.1
Hf	3.4	3.2	3.7	3.3	3.4	3.6	3.3	3.8	3.8	3.6	3	3.3	3.6	3.4	3.6	3.2
Nb	15	14.2	18.5	16.2	15	14.3	13.9	14	13.9	13.7	16.8	19	14.9	15.5	15.6	13.3
Rb	29.1	30.9	42.2	45	29.9	28.8	26.1	25.2	29.2	27.7	24.3	31.3	34.8	30	26.2	32.4
Sr	310.7	291.1	342.5	301.5	296.7	377	318.2	362.1	368.7	359.8	345.1	360.5	316.2	321	310	292.5
Ta	1.1	1	1.3	1.3	1.2	1.1	0.9	0.9	1	0.9	1.1	1.4	1.1	1.1	1	1
Th	3.4	3.1	4.5	3.5	3.5	4	3.4	3.9	4.3	3.4	2.6	4	3	2.9	3.4	2.6
U	1	1.2	1.7	1.8	1.3	0.8	0.8	0.9	0.8	0.8	0.8	1	1	1	1	1.1
V	183	177	187	173	186	174	188	174	173	167	174	180	174	189	182	172
Zr	116.2	113.1	123.8	110.1	109	133.4	115.2	127.7	126.6	125.9	114.4	122.6	111.9	117	115.2	110.3
Y	26.7	23.3	25.9	24	25.3	28.1	24.7	27.6	25.8	26.6	23.3	24	23.5	24.3	23.8	24.9
La	16.9	15.1	17.3	15	13.8	17.2	15.6	16.7	16.6	16.6	14.8	17.3	15.6	15.1	15.6	14.2
Ce	34.3	31.8	35.9	32.1	29.7	37.1	31.2	35.6	35.9	34.8	31.6	36.9	33	33.7	32.5	30.4
Pr	4.04	3.76	4.29	3.75	3.55	4.4	4.06	4.35	4.13	4.15	3.77	4.21	3.98	3.9	3.92	3.51
Nd	19.2	18	19.9	18	16.9	21	18.6	21.6	19.2	19.3	17	19.5	17.9	18.1	17.8	16.3
Sm	4.2	4	4.3	4.1	4	4.5	4.1	4.5	4.4	4.5	3.9	4.4	4	4.3	4.5	3.9
Eu	1.53	1.39	1.42	1.33	1.41	1.56	1.54	1.58	1.58	1.54	1.42	1.55	1.36	1.32	1.38	1.32
Gd	4.9	4.51	4.79	4.55	4.54	5.16	4.89	5.14	4.97	5.21	4.72	4.59	4.48	4.58	4.88	4.5
Tb	0.82	0.76	0.83	0.77	0.78	0.86	0.79	0.9	0.87	0.85	0.75	0.83	0.76	0.75	0.81	0.76
Dy	4.53	4.11	4.62	4.43	4.26	4.66	4.58	4.87	4.82	4.64	4.3	4.42	4.44	4.26	4.42	4.43
Ho	0.88	0.78	0.82	0.78	0.84	0.96	0.83	0.91	0.9	0.89	0.78	0.8	0.82	0.86	0.82	0.82
Er	2.2	2.16	2.26	2.15	2.25	2.4	2.25	2.47	2.33	2.29	2.03	2.11	2.17	2.15	2.18	2.23
Tm	0.3	0.29	0.33	0.3	0.3	0.31	0.33	0.33	0.32	0.33	0.29	0.31	0.27	0.3	0.28	0.31
Yb	2	1.84	1.87	1.71	1.95	2.01	2.01	2.21	1.92	2.06	1.73	1.79	1.71	1.86	1.86	1.91
Lu	0.28	0.27	0.28	0.27	0.28	0.3	0.28	0.3	0.28	0.28	0.23	0.23	0.26	0.26	0.25	0.29
Pb	0.7	0.6	0.9	0.4	0.9	1.2	0.9	1.2	0.7	0.6	0.8	0.9	0.5	0.9	1.1	0.4
Ce/Pb	49	53	39.88	80.25	33	30.91	34.66	29.66	51.3	58	39.5	41	66	37.44	29.54	76
La/Nb	1.13	1.06	0.93	0.92	0.92	1.20	1.12	1.19	1.20	1.21	0.88	0.91	1.04	0.97	1.0	1.06
Nb/U	15	11.83	10.88	9	11.54	17.88	17.37	15.55	17.37	17.12	21	19	14.9	15.5	15.6	12.09
Dy/Yb_N	1.52	1.49	1.65	1.73	1.46	1.55	1.52	1.47	1.68	1.50	1.66	1.65	1.73	1.53	1.59	1.55

Table 1. *(Contd.)*

Sample no.	334	335	336	340	341	343	344	345	272	276	277	280	282	284	286	288
Longitude (E)	37°14’10”	37°16’48”	37°16’51”	37°18’01”	37°19’14”	37°19’18”	37°30’07”	37°30’18”	37°20’30”	37°19’28”	37°19’28”	37°19’15”	37°18’56”	37°18’52”	37°19’05”	37°18’54”
Latitude (N)	037°13’30”	037°12’21”	037°11’56”	037°11’21”	037°10’15”	037°09’45”	037°21’51”	037°21’40”	037°19’28”	037°18’38”	037°18’38”	037°18’49”	037°20’04”	037°21’13”	037°22’37”	037°23’24”
SiO_2	53.89	53.16	52.84	54.03	53.62	51.63	52.75	52.39	53.71	53.65	53.75	53.57	53.17	50.95	51.9	51.51
Al_2O_3	16.36	13.74	13.73	14.81	14.98	14.09	14.56	14.12	14.95	15.18	15.06	16.21	14.47	14.2	14.44	14.27
Fe_2O_3	10.01	10.69	10.88	10.52	10.31	12.02	11.08	10.69	10.43	10.05	10.14	10.07	10.59	12.21	11.11	11.48
MgO	3.9	7.41	7.71	5.74	5.66	8.14	5.97	7.16	5.52	4.53	4.56	4.69	6.32	7.5	6.92	7.05
CaO	8.51	7.86	7.83	8.07	8.53	7.81	8.23	8.15	8.41	7.94	7.85	8.65	8.2	8.22	8.41	8.59
Na_2O	3.62	3.1	3.02	3.39	3.29	3.08	3.12	3.06	3.23	3.59	3.58	3.42	3.32	3.22	3.25	3.12
K_2O	1.18	1.38	1.3	1.13	1.1	0.65	1.14	1.02	1.08	1.43	1.45	1.06	1.15	0.74	1.03	1
TiO_2	1.7	1.65	1.59	1.66	1.65	1.56	1.66	1.62	1.66	1.93	1.94	1.63	1.62	1.62	1.67	1.75
P_2O_5	0.25	0.26	0.25	0.23	0.24	0.18	0.26	0.25	0.24	0.33	0.33	0.21	0.25	0.24	0.23	0.27
MnO	0.11	0.12	0.13	0.12	0.12	0.13	0.13	0.13	0.12	0.12	0.12	0.12	0.12	0.14	0.13	0.13
Cr_2O_3	0.007	0.037	0.038	0.028	0.027	0.036	0.035	0.035	0.026	0.016	0.016	0.013	0.026	0.04	0.033	0.04
Total	99.94	99.93	99.95	99.94	99.94	99.96	99.95	99.95	99.79	99.78	99.9	99.96	99.95	99.81	99.95	99.93
LOI	0.4	0.5	0.6	0.2	0.4	0.6	1	1.3	0.4	1	1.1	0.3	0.7	0.7	0.8	0.7
Normative minerals																
Q	4.76	2.57	2.32	4.51	4.31	1.42	3.91	2.94	5.07	4.48	4.65	4.41	3.09	0	0	0
Or	6.99	8.17	7.7	6.69	6.51	3.85	6.75	6.04	6.39	8.47	8.58	6.27	6.81	4.38	6.1	5.92
Ab	30.63	26.23	25.55	28.68	27.84	26.06	26.4	25.89	27.33	30.37	30.29	28.94	28.09	27.24	27.5	26.4
An	24.93	19.51	20.08	21.88	22.88	22.72	22.37	21.8	23.12	21.11	20.77	25.77	21.2	22.12	21.79	22
Ne	0	0	0	0	0	0	0	0	0	0	0	0	0	0	0	0
Di	13.04	14.52	13.99	13.72	14.7	12.15	13.79	13.9	14.02	13.39	13.32	13.04	14.64	14.12	15.22	15.57
Hy	11.1	20.05	21.36	16.03	15.16	24.54	17.16	19.78	15.24	12.22	12.41	13.3	17.19	20.71	21.21	21.51
Ol	0	0	0	0	0	0	0	0	0	0	0	0	0	3.34	0.41	0.55
Mt	4.35	4.65	4.73	4.58	4.48	5.23	4.82	4.65	4.54	4.37	4.41	4.38	4.61	3.54	3.22	3.33
İl	3.23	3.13	3.02	3.15	3.13	2.96	3.15	3.08	3.15	3.67	3.68	3.1	3.08	3.08	3.17	3.32
Ap	0.59	0.62	0.59	0.55	0.57	0.43	0.62	0.59	0.57	0.78	0.78	0.5	0.59	0.57	0.55	0.64
Trace elements																
Ni	46	200	220	109	90	265	140	170	96	40	48	57	156	243	154	183
Sc	15	16	16	17	17	17	18	17	18	17	17	17	17	18	18	19
Ba	272.2	186.6	192.5	251.1	232.2	169.9	201.4	202.9	241.2	408.5	475.1	204.2	236.2	174.6	235	190.6
Co	42.5	51.4	55.2	45.8	44	55.6	48.3	48.1	46	41.1	38.9	45.7	54.7	58.4	49.4	52.6
Cs	0.8	0.8	0.9	0.8	0.7	0.5	0.9	0.7	0.7	0.7	0.7	0.5	0.8	0.3	0.5	0.4
Ga	24.3	22.8	22.4	22.7	23	22.2	22.4	20.9	22.6	23.7	23.4	23.6	21.8	22.3	22.6	21.5
Hf	3.7	3.6	3.3	3.7	3.9	2.9	3.2	3	3.1	4.3	4.5	3.4	3.7	3.1	3.5	3.6
Nb	13.7	17.9	17.6	15.2	15	10.5	16.9	16.5	13.1	22.6	23.7	11.6	15.3	14.4	13.6	17.2
Rb	31.7	41.6	43.4	27.8	25.8	14.8	30	23.2	28.2	35.8	33.6	22	33.8	16.5	21.7	21.4
Sr	372	342.7	344.8	362.9	351.3	267.1	332.2	331.5	319.3	421.5	425.3	321	319.2	307.8	324.8	346.6
Ta	1.1	1.3	1.4	1.2	1	0.8	1.2	1.3	1	1.5	1.5	0.8	1.1	1	0.9	1.2
Th	3.7	3.9	3.7	3.3	3.7	2.4	2.7	3.1	3.1	3.8	4.2	3.3	4.2	2.2	2.1	2.6
U	0.7	1.9	1.8	1	0.9	0.5	1	1	1	1.1	1.2	0.7	1.1	0.6	0.8	0.8
V	173	174	179	181	184	163	189	175	174	191	188	165	170	184	173	188
Zr	125.1	116.4	115.8	130.7	130.7	98.4	112.4	109.3	109.6	138.9	138.1	110.2	117.2	97	104.3	112.4
Y	26.4	24.7	25.5	25.8	25	22	29.5	23.4	25.7	28	28.3	25.8	25.3	23.6	23.6	23.3
La	17.1	15.9	16.3	17.7	17.9	12.5	18.9	15.7	14.2	19.9	19.8	14.1	14.7	13.5	12.9	15.1
Ce	36.8	34.9	34.3	37.5	37.6	25.6	34.2	32.6	29.3	40	40	28.8	31.4	26.6	26.4	31.4
Pr	4.25	4.16	4.03	4.35	4.39	3.14	4.53	3.86	3.81	5.1	5.03	3.62	4.04	3.52	3.48	3.95
Nd	19.3	19.4	18.3	19.7	20.2	14.9	21.3	17.7	17.4	22.2	22	16.7	18.7	16.5	16	17.6
Sm	4.7	4.3	4.1	4.4	4.5	3.6	4.5	4.1	4.4	5	5.1	4.2	4.3	4	4.1	4.2
Eu	1.54	1.47	1.38	1.46	1.48	1.26	1.5	1.36	1.42	1.66	1.64	1.53	1.52	1.42	1.42	1.46
Gd	5.09	5	4.83	4.88	5.09	4.35	5.32	4.34	4.8	5.02	5.18	4.81	4.46	4.45	4.52	4.7
Tb	0.85	0.8	0.83	0.8	0.83	0.68	0.84	0.71	0.8	0.89	0.92	0.82	0.85	0.8	0.77	0.82
Dy	4.68	4.48	4.67	4.49	4.66	3.94	4.9	4.28	4.2	4.71	4.81	4.2	4.38	4.07	4.09	4.08
Ho	0.9	0.82	0.89	0.85	0.83	0.73	0.92	0.76	0.83	0.89	0.92	0.82	0.84	0.76	0.76	0.76
Er	2.32	2.19	2.24	2.2	2.29	1.95	2.37	2.03	2.15	2.31	2.4	2.18	2.28	2.05	2.01	2.03
Tm	0.3	0.29	0.29	0.3	0.32	0.26	0.33	0.26	0.28	0.32	0.32	0.31	0.28	0.29	0.27	0.28
Yb	2.08	1.8	2.06	1.9	1.99	1.68	1.99	1.66	1.72	1.93	1.96	1.74	1.71	1.72	1.57	1.6
Lu	0.28	0.28	0.26	0.28	0.25	0.23	0.27	0.25	0.27	0.27	0.28	0.26	0.29	0.23	0.25	0.25
Pb	0.6	0.6	0.5	0.7	0.8	0.5	0.6	1	0.5	1	1.5	1.1	0.7	0.7	0.4	0.5
Ce/Pb	61.33	58.16	68.6	53.57	47	51.2	57	32.6	58.6	40	26.66	26.18	44.85	39	66	62.8
La/Nb	1.24	0.88	0.93	1.16	1.19	1.19	1.11	0.95	1.08	0.88	0.83	1.21	0.96	0.94	0.95	0.87
Nb/U	19.57	9.42	9.77	15.2	16.67	21	16.9	16.5	13.1	20.54	19.74	16.57	13.9	24	17	21.5
Dy/Yb_N	1.50	1.66	1.52	1.58	1.57	1.57	1.65	1.72	1.63	1.63	1.65	1.61	1.71	1.58	1.74	1.70

https://doi.org/10.1017/S0016756807003524 Published online by Cambridge University Press

Table 1. *(Contd.)*

Sample no.	291	295	254	256	257	258	260	263	266	267	268	269
Longitude (E)	37°18’31”	37°19’20”	37°23’57”	37°23’30”	37°23’14”	37°23’05”	37°22’48”	37°22’42”	37°23’54”	37°21’31”	37°21’20”	37°21’20”
Latitude (N)	037°25’54”	037°29’15”	037°34’19”	037°33’55”	037°33’33”	037°33’40”	037°32’58”	037°33’00”	037°32’16”	037°32’33”	037°32’38”	037°33’28”
SiO_2	53.24	52.98	49.55	49.75	52.75	52.41	50.45	52.73	50.47	52.76	51.27	51.11
Al_2O_3	13.84	14.42	13.17	13.23	13.66	13.78	14.28	13.59	14.46	14.23	13.69	13.56
Fe_2O_3	10.73	10.79	11.46	11.49	10.99	11.04	12.37	10.93	12.19	11.17	11.61	11.38
MgO	7.87	7.05	8.21	8.68	8.17	8.35	7.5	8.13	7.89	6.81	8.07	8.74
CaO	8.12	7.9	9.86	9.59	7.84	7.77	8.97	7.75	8.9	8.32	8.5	8.7
Na_2O	2.91	3.07	2.97	2.87	3.1	3.07	2.95	2.97	2.94	3.05	2.98	2.91
K_2O	1	0.86	0.73	0.78	1.1	1.1	0.78	1.12	0.75	0.73	0.77	0.76
TiO_2	1.39	1.57	1.68	1.62	1.62	1.59	1.62	1.6	1.61	1.53	1.61	1.58
P_2O_5	0.19	0.22	0.22	0.22	0.23	0.23	0.23	0.22	0.22	0.19	0.2	0.21
MnO	0.13	0.13	0.13	0.13	0.13	0.13	0.13	0.13	0.14	0.13	0.13	0.13
Cr_2O_3	0.038	0.029	0.045	0.048	0.039	0.041	0.04	0.041	0.039	0.035	0.049	0.044
Total	99.98	99.94	99.96	99.95	99.96	99.95	99.94	99.95	99.94	99.79	99.82	99.97
LOI	0.5	0.9	1.9	1.5	0.3	0.4	0.6	0.7	0.3	0.8	0.9	0.8
Normative minerals												
Q	3.45	4.12	0	0	1.78	1.27	0	1.19	0	4.17	0	0
Or	5.92	5.09	4.32	4.62	6.51	6.51	4.62	6.63	4.44	4.32	4.56	4.5
Ab	24.62	25.97	25.13	24.28	26.23	25.97	24.96	25.13	24.87	25.81	25.21	24.62
An	21.76	23.05	20.46	20.93	20.13	20.59	23.44	20.46	24.06	23.01	21.72	21.71
Ne	0	0	0	0	0	0	0	0	0	0	0	0
Di	14.08	12.08	22.14	20.64	14.08	13.42	16.16	13.61	15.39	14	15.74	16.44
Hy	21.89	20.57	10.61	12.75	22.54	23.41	18.88	25.49	18.7	19.49	23.72	21.92
Ol	0	0	8.36	8.28	0	0	4.08	0	5.06	0	1.05	3.15
Mt	4.67	4.69	3.32	3.33	4.78	4.8	3.59	3.17	3.53	4.86	3.37	3.3
İl	2.64	2.98	3.19	3.08	3.08	3.02	3.08	3.04	3.06	2.91	3.06	3
Ap	0.45	0.52	0.52	0.52	0.55	0.55	0.55	0.52	0.52	0.45	0.47	0.5
Trace elements												
Ni	210	130	268	298	268	281	232	261	228	201	272	296
Sc	17	17	18	19	17	17	20	17	20	18	18	18
Ba	145.7	314.6	162	168.3	193.8	183.4	175.1	198	178.1	367.5	157.8	155
Co	54.7	52	54.5	60.5	55.7	60.9	56.9	56.8	59.3	53.6	56.6	55
Cs	0.9	0.4	0.4	0.5	0.4	0.5	0.5	0.4	0.4	0.3	0.5	0.3
Ga	20.1	21.5	22.1	20.9	22	21.7	22.3	21	21.3	21.8	20.4	19.8
Hf	3.3	3.8	2.9	3	3.6	3.6	3	3.2	3	2.9	3.1	3
Nb	11.3	12.4	15.8	14.6	15	14.7	13.7	14.7	13.5	10.9	13.9	11.9
Rb	30.5	18	16.9	19.9	24.7	26.6	18.2	28.5	15.9	16.5	20.3	14.3
Sr	264	315.9	324.5	319.7	328.2	343.6	320.9	333	318.6	296.6	309.5	277.8
Ta	0.8	0.8	1.1	1	0.9	1	1	1	0.9	0.8	1	0.8
Th	2.7	2.6	2.5	2.6	3.7	2.5	1.8	2.9	1.6	2.8	2.4	2.5
U	1.2	0.7	0.5	0.7	0.9	0.8	0.6	0.9	0.5	0.6	0.6	0.6
V	164	170	178	188	172	173	192	166	194	163	174	165
Zr	94.2	112.2	105.7	102.7	114.8	113.7	101.5	111.2	102	92.9	98.9	97.2
Y	23.5	23.9	22.5	22.5	24.8	24.1	22.6	23.7	22.6	24.8	22.1	22.3
La	11.5	13.8	13.5	13.3	14.9	14.5	13	13.8	13	10.9	12.9	11.3
Ce	24.3	28.7	27.7	27.5	30.1	29.3	26.6	28.5	26.8	22	26.1	23.9
Pr	3.09	3.77	3.66	3.46	3.88	3.76	3.56	3.8	3.49	2.95	3.44	3.18
Nd	15	17.7	16.7	16.3	18.1	17.1	16.2	17.3	16.8	13.8	15.7	14.8
Sm	3.8	4.1	4	4.1	4.4	4.1	3.9	4.3	3.8	3.6	4	3.8
Eu	1.25	1.52	1.42	1.36	1.45	1.38	1.41	1.4	1.47	1.29	1.4	1.38
Gd	4.08	4.41	4.63	4.06	4.69	4.5	4.05	4.36	4.2	4.29	4.33	4.08
Tb	0.73	0.78	0.74	0.73	0.83	0.77	0.75	0.76	0.73	0.72	0.76	0.77
Dy	3.88	4.1	4.04	3.86	4.2	4.27	3.88	3.96	3.71	3.86	3.94	3.79
Ho	0.78	0.79	0.78	0.73	0.79	0.76	0.72	0.76	0.74	0.79	0.76	0.72
Er	2.06	2.07	1.91	1.94	2.18	2	1.88	1.94	1.96	2.04	1.97	1.91
Tm	0.28	0.29	0.26	0.27	0.3	0.28	0.26	0.27	0.25	0.29	0.27	0.26
Yb	1.86	1.71	1.59	1.61	1.76	1.67	1.57	1.55	1.52	1.7	1.45	1.44
Lu	0.24	0.26	0.22	0.22	0.26	0.23	0.22	0.24	0.21	0.24	0.24	0.2
Pb	0.5	1.1	0.7	0.3	0.5	0.4	0.6	0.3	0.7	0.6	0.4	0.7
Ce/Pb	48.6	26.1	39.57	91.66	60.2	73.25	44.33	95	38.28	36.66	65.25	34.14
La/Nb	1.02	1.11	0.85	0.91	0.99	0.98	0.95	0, 93	0.96	1.0	0.93	0.95
Nb/U	9.41	17.71	31.6	20.85	16.67	18.37	22.83	16.33	27	18.16	23.16	19.83
Dy/Yb_N	1.4	1.6	1.7	1.6	1.6	1.71	1.65	1.70	1.63	1.52	1.81	1.76

*Major and trace elements are given in wt % and ppm, respectively.

reveals the within-plate character of the early–middle Miocene volcanic rocks (Fig. 6). On primitive mantle-normalized plots, the basalt data form subparallel patterns with a pronounced depletion in Pb, and a slight depletion at Nb–Ta (Fig. 7a). Primitive mantle-normalized REE plots show their slightly enriched nature in LREE, with resulting La/Yb_N ratios between 5.47 and 6.71 (Fig. 7b). The absence of negative Eu anomalies in the REE-normalized plot indicates no or insignificant plagioclase fractionation.

5. Discussion

Compositions of continental basalts are controlled by source composition, degree of partial melting, magma mixing and shallow processes such as crustal contamination and crystal fractionation. The relative importance of these parameters and processes in the generation of early–middle Miocene volcanic rocks will be explored in this section. Based on petrogenetic interpretation, a geodynamic consideration is developed to account for the flood basalt occurrence in Southeast Anatolia.

5.a. Fractional crystallization

Olivine, plagioclase, clinopyroxene and oxides are observed in all samples and are probably the main phases which fractionate. Between 9 % and 7 % MgO, the CaO contents in the early–middle Miocene volcanic rocks decrease significantly from 10 % to 8 % (Fig. 4). This variation is probably due to low-pressure fractionation of clinopyroxene (?). They show a coherent fractionation trends from basalt to basaltic andesites. The phenocryst assemblages observed in the early–middle Miocene volcanic rocks suggest that variable fractionation of olivine + clinopyroxene and plagioclase occurred. Major element variations against MgO contents in Figure 4 support olivine + clinopyroxene fractionation. In thin-section, plagioclase appears to be an important fractionating phase, particularly in evolved rocks. However, plagioclase fractionation is not supported by increasing Al_2O_3 with decreasing MgO (Fig. 4).

Pearce Element Ratio (PER) diagrams (Nicholls, 1988; Russell & Nicholls, 1988) have been used to explain some of the processes which contributed to the chemical variation among the samples. The PER diagrams with 0.5(Fe + Mg) v. Si and 2Ca + 3Na v. Si (Fig. 8) were used to test for the fractionation of plagioclase and/or clinopyroxene, and plagioclase and/or olivine or orthopyroxene. Early–middle Miocene volcanic rocks produce two lines with distinct slopes on diagrams which differentiate between clinopyroxene and olivine, that is, 0.5(Fe + Mg) v. Si (Fig. 8a). They produce two lines with the same slopes, implying plagioclase fractionation (Fig. 8b). The plot of (0.25 Al + 0.5(Fe + Mg) + 1.5 Ca + 2.75 Na)/K v. Si/K produce a trend with a slope of one; the chemical variations in the data can be explained by fractionation of olivine, plagioclase and clinopyroxene in any combination (Fig. 8c).

5.b. Effects of crustal contamination

Lavas erupted through continental lithosphere can be contaminated with relatively high-SiO_2 crustal material en route to the surface. Therefore, the continental crust has the potential to modify their composition. Crustal assimilation is responsible for some of the compositional effects, for example, incompatible trace element shifts. It has been commonly believed that the continental tholeiites have distinctive negative Nb and Ta anomalies with respect to normalized trace-element patterns (Cox & Hawkesworth, 1985). In addition, continental crust has been characterized by highly fractionated and enriched LREE, flat HREE, positive Pb but negative anomalies at Nb–Ta (Taylor & McLennan, 1985). The effect of crustal contamination on lava compositions is most readily apparent in major and trace element data. Relatively Si-rich samples tend to have high K/Nb, Ba/La and U/Pb ratios, and lower Ce/Pb and Dy/Yb_N ratios (Table 1). Primitive mantle-normalized trace element patterns show a slightly negative anomaly at Ta–Nb (Fig. 7a). To further evaluate the crustal material involved in the early–middle Miocene flood basalts, incompatible trace element ratios, which are relatively insensitive to moderate to large degrees of partial melting and to fractional crystallization processes, were used. The presence of continental materials in the early–middle Miocene volcanic rocks is evident in Figure 9. A Th/Yb v. Ta/Yb plot (Fig. 9a) shows a marked shift toward high Th/Yb ratios indicating crustal assimilation. In addition, the majority of the samples exhibit elevated Th/Ta_N, but La/Nb_N is close to unity in Figure 9b in that many lavas have Th/Ta_N and $La/Nb_N > 1$ (Fig. 9b). Some estimates of average upper crust composition have Th/Ta_N and $La/Nb_N > 1$ (e.g. Weaver & Tarney, 1984; Rudnick & Fountain, 1995). Figure 9 clearly suggests that the magmas have been slightly affected by upper crustal material.

5.c. Magma depth and source

It is possible to place some constraints on the depth of origin by considering the major element chemical composition of the magma. Depth of origin of basalts has an effect on the FeO*, MgO and SiO_2 contents of magma (Langmuir, Klein & Plank, 1992; Kushiro, 1996) and on the degree of silica undersaturation of the magmas (Takahashi & Kushiro, 1983; Green, 1971; Kushiro, 1996). Kushiro (1996) suggested that the liquids in equilibrium with fertile mantle peridotite at pressures less than 10 kbar have normative hypersthene regardless of melt fraction. At 15 kbar and above, the liquids are nepheline-normative for melt fractions

https://doi.org/10.1017/S0016756807003524 Published online by Cambridge University Press

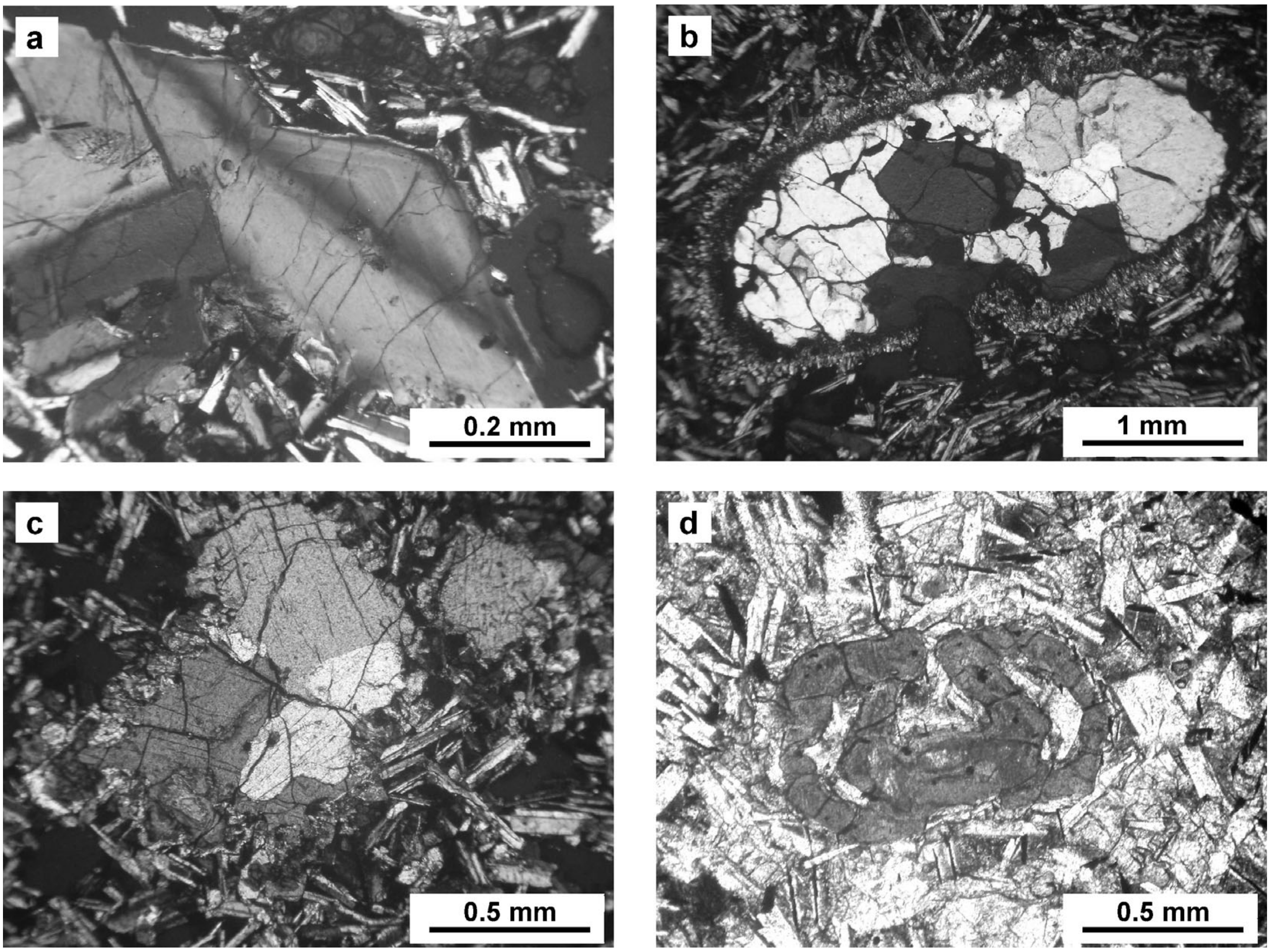

Figure 3. (a) Plagioclase with zoning pattern (plane polarized light, sample 326); (b) quartz xenocryst with clinopyroxene rim (plane polarized light, sample 246); (c) clinopyroxene glomerocrysts surrounded by olivine (plane polarized light, sample 245); (d) skeletal olivine (parallel light, sample 319); (e) resorbed olivine (parallel light, sample 248); (f) rounded olivine microphenocrysts (parallel light, sample 271); (g) olivine phenocryst including rounded melt inclusion (parallel light, sample 292); (h) dendritic olivine growth (parallel light, sample 297).

smaller than about 10 %, but hypersthene-normative for larger melt fractions at lower pressures (DePaolo & Daley, 2000). All basaltic samples are hypersthene-normative, except one sample, implying that the magmas resulted from larger degrees of melting at lower pressures (Table 1). These data may indicate that the melts were formed in the spinel-peridotite field, although a garnet-peridotite source cannot be excluded. These arguments are also supported by the REE constraints in Figure 11. Figure 11 indicates that the melts come from both garnet- and spinel-peridotite sources with a higher degree of melting (> 5 % in garnet-peridotite and > 10 % in spinel-peridotite). These data imply that the depth of melting changes from spinel-peridotite to garnet-peridotite fields.

To evaluate the different components involved in flood basaltic volcanism in South Anatolia, the incompatible element ratios can be used. The element ratios used are relatively insensitive to partial melting and to fractional crystallization processes, and thus should approximately represent source compositions. In the plot of Nb/Y–Zr/Y, early–middle Miocene volcanic rocks of the Southeast Anatolia plot in the Icelandic mantle array (Fig. 10). Although all the samples with < 53 % SiO_2 have an OIB-like characterization (Fig. 7), their continental setting requires melts originated from lithospheric mantle or asthenospheric mantle. During the extension of the lithosphere, deeper parts of the mantle ascend and melt adiabatically (McKenzie & Bickle, 1988); thus, both deep lithospheric mantle and the asthenosphere are possible magma sources. Lithospheric mantle has a high and variable degree of La/Nb, which is generally higher than 1, whereas the asthenospheric magma source has a low, well-defined ratio of La/Nb (0.7) (DePaolo & Daley, 2000). La/Nb values of the samples with < 52 % SiO_2 are lower than 1, varying from 0.79 to 0.96, except those of sample no. 343, which has an La/Nb ratio of 1.19. A combination of this information with OIB-like trace-element patterns for the early–middle Miocene volcanic rocks indicates that melts have originated in the asthenospheric mantle rather than lithospheric mantle.

https://doi.org/10.1017/S0016756807003524 Published online by Cambridge University Press

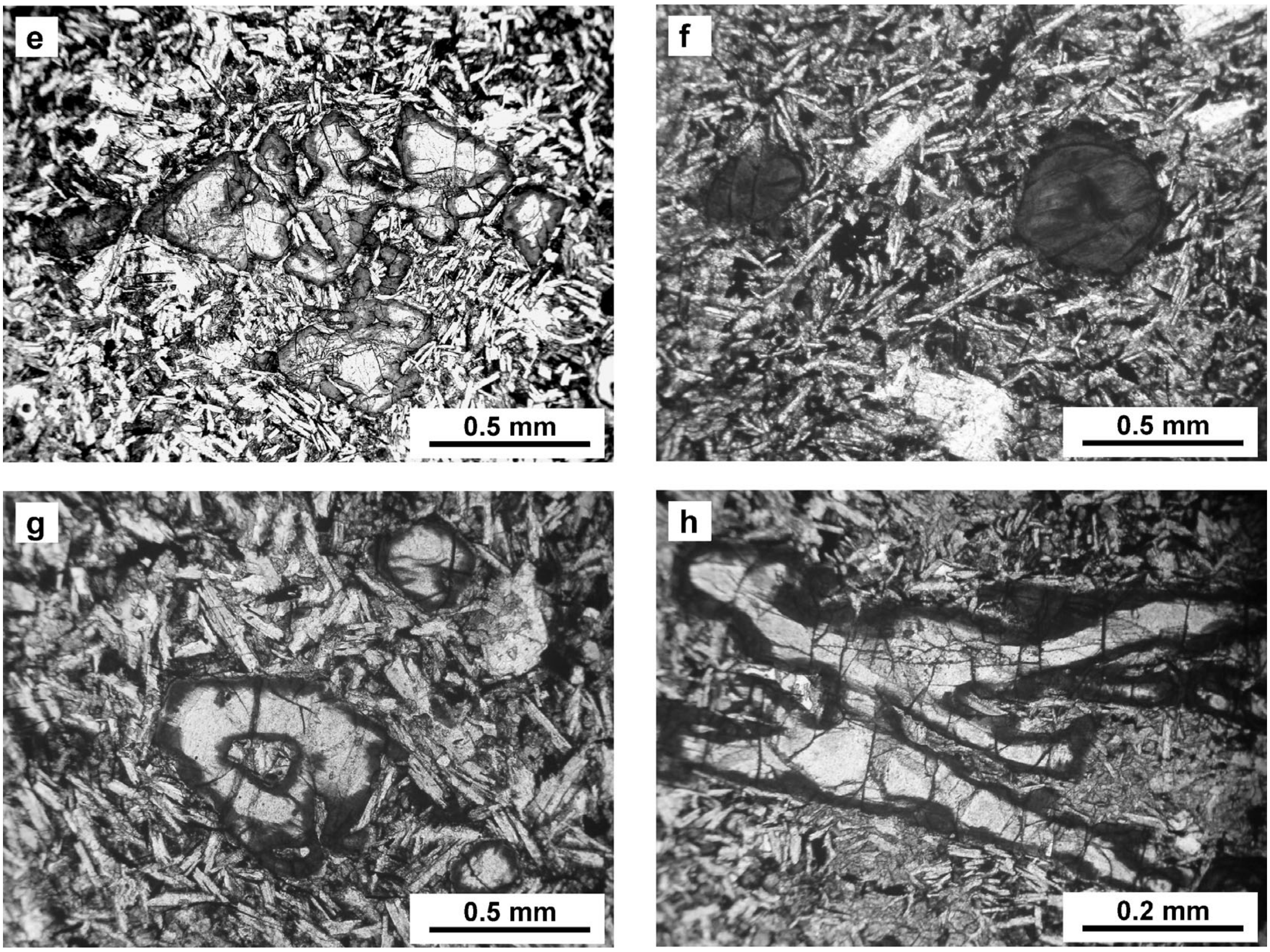

Figure 3. Contd.

5.d. Partial melting constraints from rare earth elements

Rare earth element ratios are useful for constraining partial melting, along with the chemical and mineralogical characteristics of the source and melting depth (McKenzie & O'Nions, 1991; Ellam, 1992; Fram & Lesher, 1997; Shaw *et al.* 2003). The utility of the REEs in this regard derives mostly from their dramatic change in partitioning during melting of garnet-peridotites versus spinel-peridotites (Wang *et al.* 2002). This is because solid:melt partitioning of REE is different for spinel- and garnet-peridotite. Partial melting of either a spinel- or garnet-peridotite will preferentially enrich the LREE in the melt and produce La/Yb variations with variable degrees of partial melting, although the La/Yb variations will have a wide range, if melting occurs in garnet-peridotite rather than spinel-peridotite. The degree of enrichment of MREE to HREE depends on whether garnet exists as a residual phase during partial melting, as HREE retained by garnet during melting (high $D_{Yb} \sim 4.0$–15.0) relative to MREE (McKenzie & O'Nions, 1991). This produces large variations in MREE/HREE ratios in melts formed by partial melting of garnet-peridotite, and there are large differences between source and melt ratios. In contrast, if partial melting of a spinel-peridotite occurs, it will produce little variation in MREE/HREE ratios with melt, and their source and melt ratios will be similar. Correlations between LREE/HREE (e.g. La/Yb) and MREE/HREE (e.g. Dy/Yb) will be linear when two melts of different REE composition are mixed, as the same element is used as a denominator of both ratios.

Figure 11 presents La/Yb_N versus Dy/Yb_N data for the early–middle Miocene volcanic rocks, along with trajectories of non-modal batch melts of garnet- and spinel-peridotite sources. Source concentrations use the primitive mantle values of Sun & McDonough (1989), which is only a crude approximation of the likely source concentration. Variable degrees of partial melting of a spinel-peridotite source cannot produce the observed variation in La/Yb_N and Dy/Yb_N, as melts derived from a spinel-peridotite source do not have co-variation of La/Yb with Dy/Yb to produce early–middle Miocene volcanic rocks, nor do they have sufficiently high Dy/Yb to produce the high Dy/Yb values of many samples (Fig. 11). Variable degrees of partial melting of a garnet-peridotite cannot account for the La/Yb_N–Dy/Yb_N variation in Figure 11,

https://doi.org/10.1017/S0016756807003524 Published online by Cambridge University Press

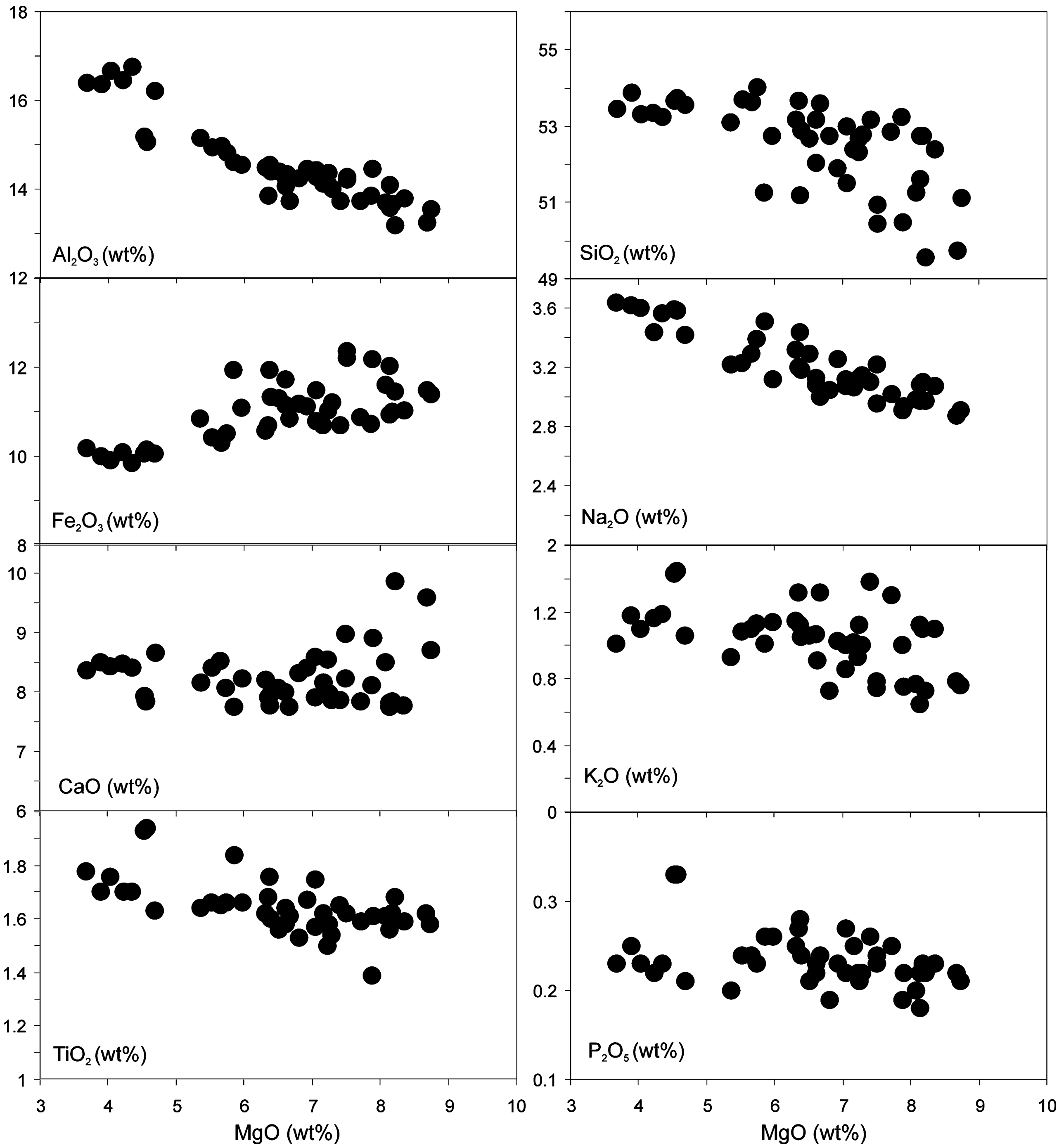

Figure 4. Major element variations plotted against MgO.

as the lowest Dy/Yb ratios of the early–middle Miocene volcanic rocks require unrealistically large degrees of partial melting of the garnet-peridotite source (> 25 %). These arguments imply that the melts were not originated from a single source material, either spinel- or garnet-peridotite. Partial melting modelling shown in Figure 11 requires interaction of melts derived from both garnet- and spinel-peridotite sources. Basaltic samples of the early–middle Miocene volcanic rocks fall on the binary mixing line, which is calculated between low-degree melt (< 5 %) from a garnet-peridotite source and high-degree melt (> 10 %) from a spinel-peridotite source.

5.e. Magma mixing

Partial melting of a single mantle source is also difficult to reconcile with partial melting modelling based on REE data. Figure 11 indicates the presence of both spinel- and garnet-peridotite as a source material. Furthermore, REE modelling requires binary melt mixing for early–middle Miocene volcanic rocks, as

https://doi.org/10.1017/S0016756807003524 Published online by Cambridge University Press

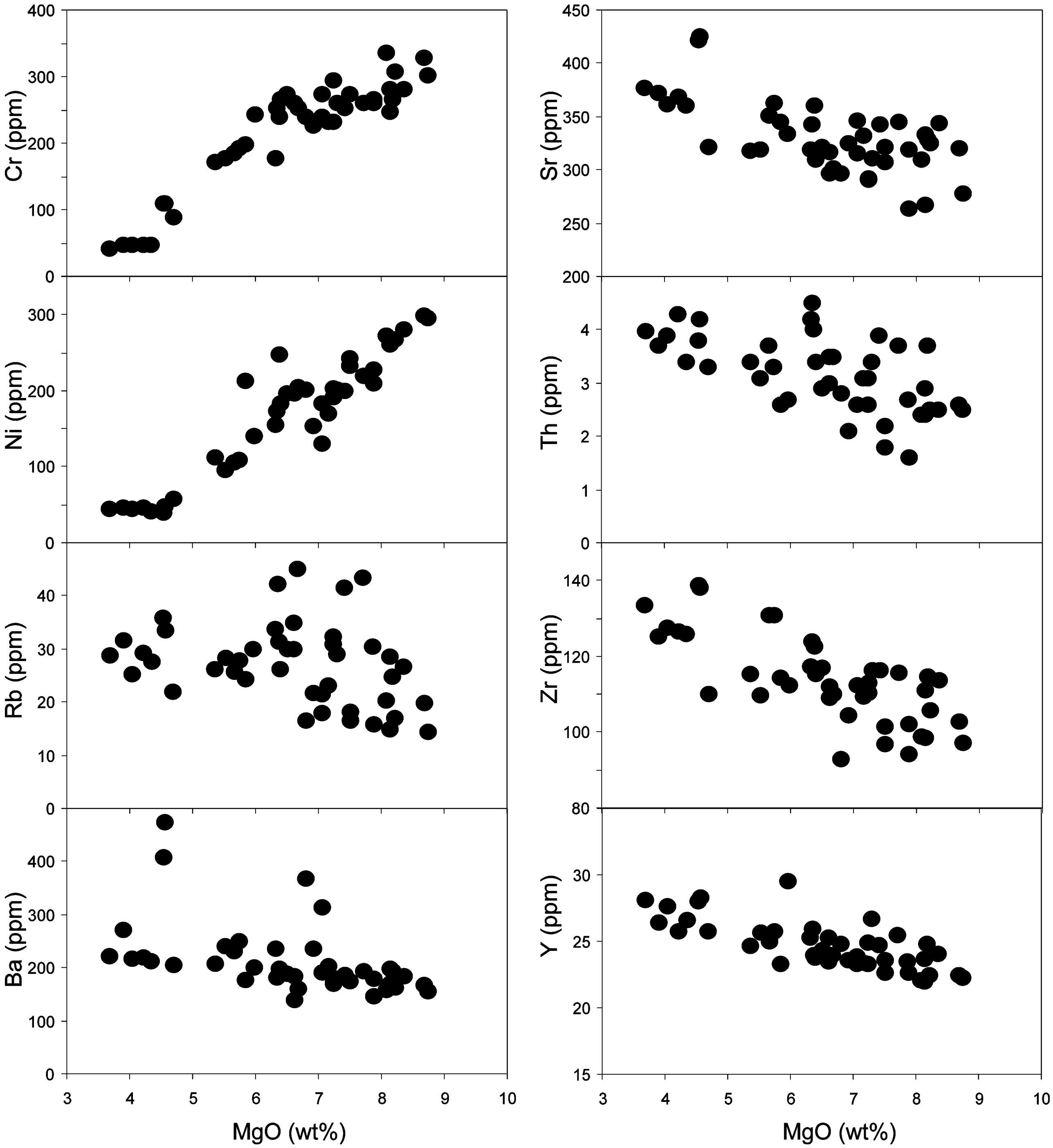

Figure 5. Some compatible and incompatible trace element variations plotted against MgO.

outlined above (Fig. 11). Further evidence for mixing between melts that originated from distinct sources can be found in petrographic features, particularly in olivine morphologies. Despite the refractory nature of olivine, chemical and/or thermal disequilibrium between olivine and host melts is not uncommon in nature and results in partial olivine resorption. Early–middle Miocene volcanic rocks contain rounded and embayed olivine phenocrysts (0.5–5 mm) with smaller euhedral and skeletal phenocrysts of olivine which have been interpreted as the mixing of compositionally distinct magmas (Richter & Murata, 1966; Wright, 1973; Gerlach & Grove, 1983) (Fig. 3). Some olivine phenocrysts contain abundant and elongated melt inclusions (Fig. 3d). These features require olivine dissolution in melts in which it is unstable as a result of the mixing of olivine into hotter magma or compositionally incompatible magma. These conditions are exemplified by the dynamic convection of a magma that crystallizes olivine and circulates it to hotter regions, the mixing of olivine-bearing melts of dissimilar composition or temperature,

https://doi.org/10.1017/S0016756807003524 Published online by Cambridge University Press

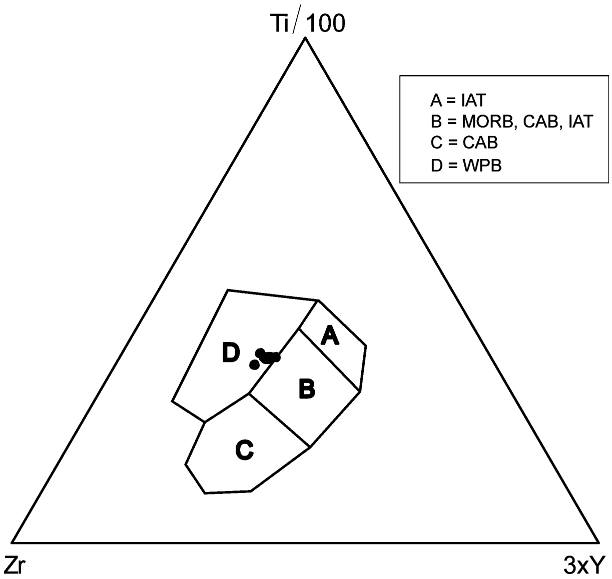

Figure 6. Ti–Zr–Y discrimination plot of Pearce & Cann (1973) for the studied basalts.

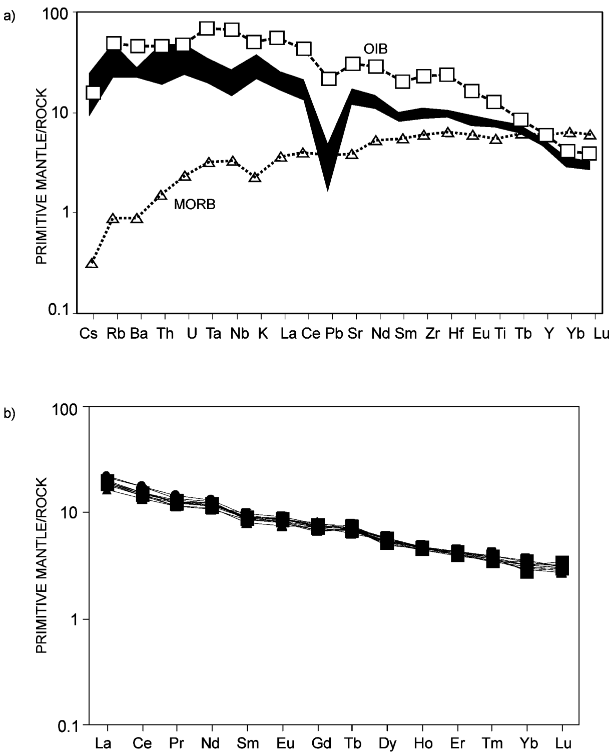

Figure 7. Primitive mantle-normalized trace element (a) and REE (b) diagram for basalts. Normalized values from Sun & McDonough (1989).

and the reaction of olivine with the fractionated product of its own parent magma (Thornber & Huebner, 1985). Data from morphological features of olivine (Fig. 3) and partial melting modelling (Fig. 11) suggest that the melts forming early–middle Miocene volcanic rocks are interpreted as having been derived from two separate sources, of which one is a spinel-peridotite and the other a garnet-peridotite. Melts originated from

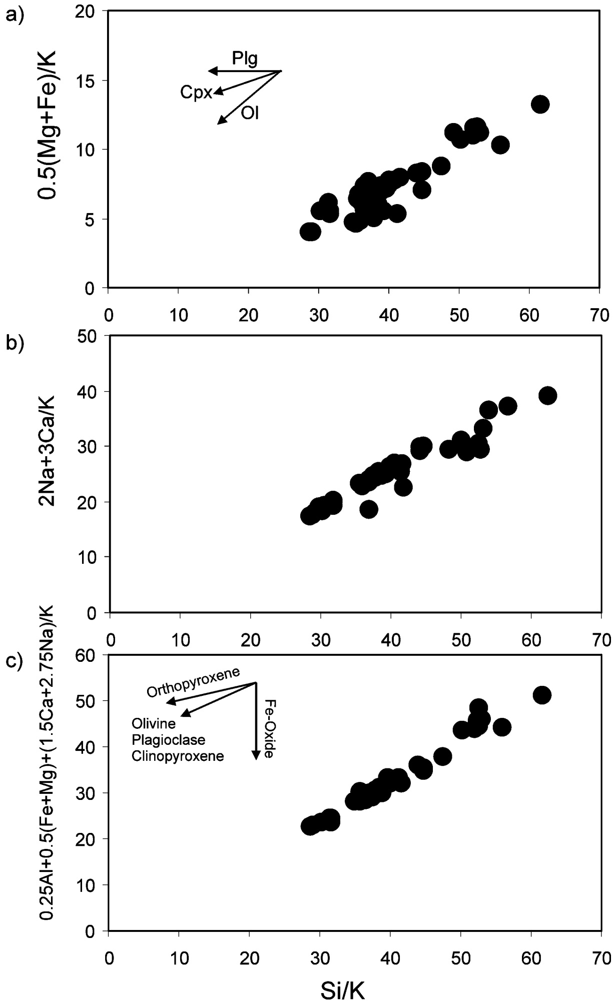

Figure 8. PER diagrams for the studied volcanics using K as a denominator. (a) 0.5(Fe + Mg) v. Si, (b) 2Na + 3Ca v. Si and (c) (0.25Al + 0.5(Fe + Mg) + 1.5Ca + 2.75Na) v. Si.

these sources were initially tapped by spatially distinct magma chambers, which subsequently coalesced into a single flow of blended melt. It can be presumed that resorption of olivine phenocrysts originally present in one of the source magmas resulted from the thermal and compositional incompatibility of this olivine with the hybridized host melt.

6. Geodynamic considerations

The Neogene tectonic evolution of Southeast Anatolia has been largely influenced by the collision of the African and Arabian plates with the Eurasian plate. Northward subduction of the southern Tethys between Anatolia and the Arabian platform is responsible for the Bitlis–Zagros orogeny during middle Miocene times (Perinçek, 1979; Yazgan *et al.* 1983; Dewey *et al.* 1973; Şengör & Kidd, 1979; Yılmaz, 1993). Hempton (1985) documented the Middle to Late Eocene as the initial period of final collision on the northern Arabian margin. After the Middle to Late Eocene

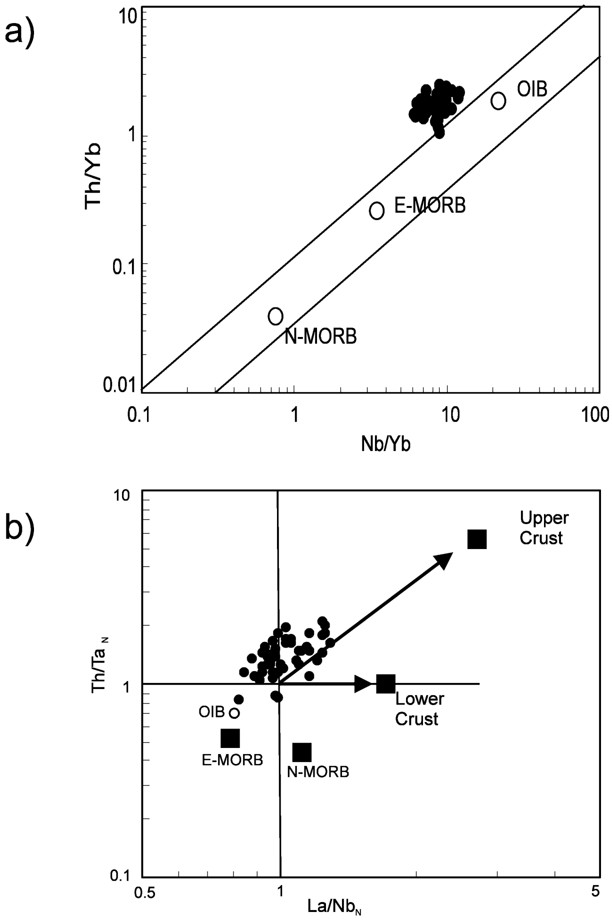

Figure 9. (a) Th/Yb v. Nb/Yb and (b) Th/Ta_N v. La/Nb_N plots for studied volcanic rocks.

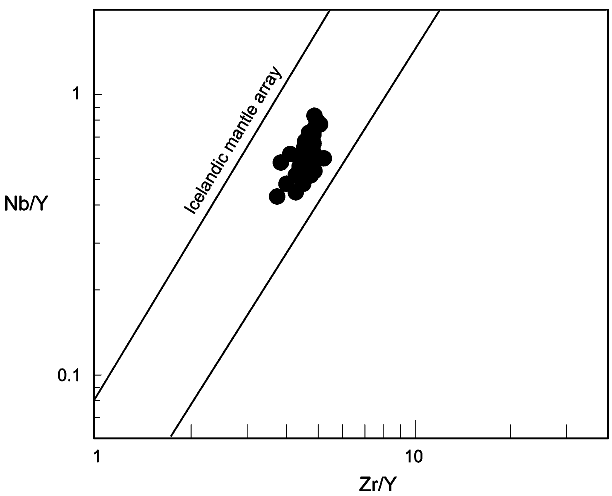

Figure 10. Nb/Y–Zr/Y plot of Fitton *et al.* (1997) indicating asthenospheric source for the studied volcanic rocks.

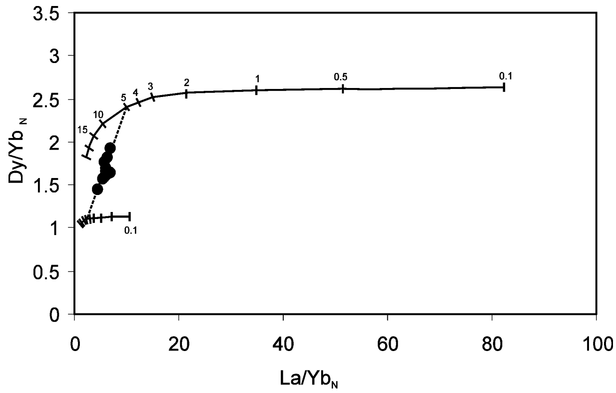

Figure 11. Calculated La/Yb_N v. Dy/Yb_N partial melting curves assuming non-modal fractional melting of garnet- and spinel-peridotite sources (garnet-peridotite: 0.598 ol, 0.211 opx, 0.076 cpx, 0.115 gr that melts in the proportions 0.05 ol, 0.2 opx, 0.3 cpx, 0.45 grt; spinel-peridotite: 0.578 ol, 0.27 opx, 0.119 cpx, 0.033 sp that melts in the proportions 0.1 ol, 0.27 opx, 0.5 cpx, 0.13 sp (Thirlwall, Upton & Jenkins, 1994); partition coefficients from the compilation of McKenzie & O'Nions, 1991). Dashed line represents mixing of partial melts from spinel- and garnet-peridotite mantle.

suturing of Africa/Arabia to Eurasia, convergence between the plates was partially accommodated by the shortening and thickening of the Arabian continental margin (Hempton, 1985). The stress created by this ongoing convergence continued the formation of the compressional features that began forming in Middle to Late Eocene times. This stress regime was changed by the Late Oligocene/Early Miocene initiation of continental stretching and rifting in the Red Sea. Rifting in the Red Sea led to the first phase of motion along the southern Dead Sea Fault Zone (Hempton, 1987). Initiation of the Dead Sea Fault Zone and opening of the Red Sea (Gaulier *et al.* 1988) caused the separation of the Arabian plate from Africa, and its northward migration (Le Pichon & Gaulier, 1988). The Dead Sea Fault Zone runs from the Red Sea to the Bitlis belt at the Maraş triple junction, and it acted as a complex left-lateral intracontinental transform between the Red Sea accretion and the Bitlis collision (Adıyaman & Chorowicz, 2002). The African–Arabian divergent plate movement and opening of the Red Sea are the principal factors that influenced the structural development in SE Turkey.

Studies on tectonics of southern Turkey indicate that some faults have been linked to the Dead Sea Fault Zone (Coşkun, 1998, 2004; Westaway, 2003; Westaway *et al.* 2006). Neogene faults in the study area are composed of splays of the Dead Sea Fault Zone (Coşkun, 2004). These faults originally developed as a result of the latest Cretaceous ophiolite obduction (Tolun & Pamir, 1975) and were reactivated in Neogene times (Terlemez *et al.* 1997; Coşkun & Coşkun, 2000; Yurtmen & Westaway, 2001). These Miocene faults arrive at the surface and abundant basaltic flows expand on the surface north of the Gaziantep area (Coşkun, 1998). Transtensional tectonic movements along the Dead Sea Fault Zone, which led to lithospheric extension, may have allowed partial melting as a consequence of upper mantle decompression (Lustrino & Sharkov, 2006). Close relationships between basaltic flows and the Neogene faults imply that the basaltic volcanism may be interpreted as a strong control by lithospheric discontinuities representing preferential pathways for uprising magmas in early–middle Miocene times. Therefore, it can be suggested that the magma occurs because of decompression, as a consequence of lithospheric extension relating to transtensional tectonics along the Dead Sea Fault Zone and the Neogene faults have acted to guide the melts to the surface.

7. Conclusions

Early–middle Miocene basaltic volcanism occurs in a widespread area just south of the Bitlis–Zagros collisional belt that resulted from collision of the Arabian and Eurasian plates. These basalts have a tholeiitic character based on major element data. Petrographic evidence and PER diagrams suggest olivine, plagioclase and clinopyroxene fractionation in the evolution of the melts. Slightly negative Nb–Ta anomalies and Th/Ta_N v. La/Nb_N diagrams indicate that the crustal contribution is minor but cannot be excluded. REE modelling implies mixing between low-degree melt from the garnet-peridotite mantle and high-degree melt from the spinel-peridotite mantle. Melt mixing between two contrasting melts is also supported by olivine morphologies such as skeletal, rounded and dendritic olivine phenocrysts with abundant melt inclusions.

Neogene tectonic evolution of Southeast Anatolia has largely been affected by collision between the Arabian and Eurasian plates, and by the opening of the Red Sea, which led to the formation of the Dead Sea Fault Zone. Transtensional tectonics along the Dead Sea Fault Zone may have caused partial melting due to decompression. Strike-slip faults linking to the Dead Sea Fault Zone facilitated the transport of the melts to the surface with only minor crustal contamination.

Acknowledgements. This study was supported by TUBITAK in a research grant (CAYDAG-103Y141). The author thanks TUBITAK for their financial support. The author also thanks Prof. Abidin Temel (Hacettepe University) for his helpful discussions and reviews of early versions of the manuscript.

References

ADIYAMAN, O. & CHOROWICZ, J. 2002. Late Cenozoic tectonics and volcanism in the northwestern corner of the Arabian plate: a consequence of the strike-slip Dead Sea fault zone and the lateral escape of Anatolia. *Journal of Volcanology and Geothermal Research* **117**, 327–45.

ALICI, P., TEMEL, A., GOURGAUD, A., VIDAL, P. & GÜNDOĞDU, M. N. 2001. Quaternary tholeiitic to alkaline volcanism in the Karasu valley, Dead Sea rift zone, southeast Turkey: Sr–Nd–Pb–O isotopic and trace-element approaches to crust-mantle interaction. *International Geology Review* **43**, 120–38.

ANDERSON, D. L. 1994. The sublithospheric mantle as the source of continental flood basalts; the case against the continental lithosphere and plume head reservoirs. *Earth and Planetary Science Letters* **123**, 269–80.

ARGER, J., MITCHELL, J. & WESTAWAY, R. 2000. Neogene and Quaternary volcanism of south-eastern Turkey. In *Tectonics and Magmatism of Turkey and the Surrounding Area* (eds E. Bozkurt, J. A. Winchester & J. D. A. Piper), pp. 459– 87. Geological Society of London, Special Publication no. 173.

ARNDT, N. T. & CHRISTIENSEN, U. 1992. Role of lithospheric mantle in continental volcanism: thermal and geochemical constraints. *Journal of Geophysical Research* **97**, 10967–81.

BERTRAND, H., CHAZOT, G., BLICHERT-TOFT, J. & THORAL, S. 2003. Implications of widespread high-μ volcanism on the Arabian Plate for Afar mantle plume and lithosphere composition. *Chemical Geology* **198**, 47–61.

CAMPBELL, I. H. & GRIFFITHS, R. W. 1990. Implications of mantle plume structure for the evolution of flood basalts. *Earth and Planetary Science Letters* **90**, 79–93.

COX, K. G. & HAWKESWORTH, C. J. 1985. Geochemical stratigraphy of the Deccan Traps at Mahabaleshwar, Western Ghats, India, with implication for open system processes. *Journal of Petrology* **26**, 355–87.

COŞKUN, B. 1998. New observations on the inorganic origin of petroleum and implications on the explorations in SE Turkey. *Proceedings of 12th Turkish Petroleum Congress, October 1998 Ankara, Turkey*, 259–87.

COŞKUN, B. 2004. Arabian-Anatolian Plate Movements and Related Trends in Southeast Turkey's Oilfields. *Energy Sources* **26**, 987–1003.

COŞKUN, B. & COŞKUN, B. 2000. The Dead Sea Fault and related subsurface structures, Gaziantep Basin, southeast Turkey. *Geological Magazine* **137**, 175–92.

ÇAPAN, U. Z., VIDAL, P. & CANTAGREL, J. M. 1987. K–Ar, Nd, Sr and Pb isotopic study of Quaternary volcanism in Karasu Valley (Hatav), N-end of Dead-Sea Rift zone in SE Turkey. *Yerbilimleri* **14**, 165–78.

DE PAOLO, D. J. & DALEY, E. E. 2000. Neodymium isotopes in basalts of the southwest basin and range and lithospheric thinning during continental extension. *Chemical Geology* **169**, 157–85.

DEWEY, J. F., PITMAN, W. C., RYAN, W. B. F. & BONNIN, J. 1973. Plate tectonics and the evolution of the Alpine System. *Geological Society of America Bulletin* **84**, 3137–80.

ELLAM, R. M. 1992. Lithospheric thickness as a control on basalt geochemistry. *Geology* **20**, 153–6.

ELLAM, R. M. & COX, K. G. 1989. A Proterozoic lithospheric source for Karoo magmatism: evidence from the Nuanetsi picrites. *Earth and Planetary Science Letters* **92**, 207–18.

ELLAM, R. M. & COX, K. 1991. An interpretation of Karoo picrite basalts in terms of interaction between asthenospheric magmas and the mantle lithosphere. *Earth and Planetary Science Letters* **105**, 330–42.

FITTON, J. G., SAUNDERS, A. D., NORRY, M. J., HARDARSON, B. S. & TAYLOR, R. N. 1997. Thermal and chemical structures of the Iceland plume. *Earth and Planetary Science Letters* **153**, 197–208.

FRAM, M. S. & LESHER, C. E. 1997. Generation and polybaric differentiation of east Greenland early Tertiary flood basalts. *Journal of Petrology* **38**, 231–75.

GARFUNKEL, Z. 1981. Internal structure of the Dead Sea leaky transform (rift) in relation to plate kinematics. *Tectonophysics* **80**, 81–108.

GARFUNKEL, Z. 1989. Tectonic setting of Phanerozoic magmatism in Israel. *Israel Journal of Earth Sciences* **38**, 51–74.

GAULIER, J. M., Le PICHON, X., LYBERIS, N., AVEDIK, F., GELI, L., MORETTI, I., DESCHAMPS, A. & HAFEZ, S. 1988. Seismic study of the crust of northern Red Sea and Gulf of Suez. *Tectonophysics* **153**, 55–88.

GERLACH, D. C. & GROVE, T. L. 1983. Petrology of Medicine Lake highlands volcanics: Characterization of end-members of magma mixing. *Contributions to Mineralogy and Petrology* **80**, 147–59.

GIANNERINI, G., CAMPREDON, R., FERAUD, G. & ABOU ZAKHEM, B. 1988. Déformations intraplaques et volcanisme associé: exemple de la bordure NW de la plaque arabique au Cénozoique. *Bulletin de la Société de Géologique de France* **8**, 937–47.

GREEN, D. H. 1971. Composition of basaltic magmas as indicators of conditions of origin: application to oceanic volcanism. *Philosophical Transactions Royal Society London* **A268**, 707–25.

HEIMANN, A. & RON, H. 1993. Geometric changes of plate boundaries along part of the northern Dead Sea transform: geochronologic and paleomagnetic evidence. *Tectonics* **12**, 477–91.

HEMPTON, M. 1985. Structure and deformation of the Bitlis suture near Lake Hazar, southeastern Turkey. *Geological Society of America Bulletin* **96**, 233–43.

HEMPTON, M. R. 1987. Constraints on Arabian plate motion and extensional history of the Red Sea. *Tectonics* **6**, 687–705.

HOFMANN, A. W., JOCHUM, K. P., SEUFERT, M. & WHITE, M. W. 1986. Nb and Pb in oceanic basalts: new constraints on mantle evolution. *Earth and Planetary Science Letters* **79**, 33–45.

ILANI, S., HARLAVAN, Y., TARAWNEH, K., RABBA, I., WEINBERGER, R., IBRAHIM, K., PELTZ, S. & STEINITZ, G. 2001. New K–Ar ages of basalts from the Harrat Ash Shaam volcanic field in Jordan: implications for the span and duration of the upper-mantle upwelling beneath the western Arabian plate. *Geology* **29**, 171–4.

IRVINE, T. N. & BARAGAR, W. R. A. 1971. A guide to the chemical classification of the common volcanic rocks. *Canadian Journal of Earth Sciences* **8**, 523–48.

KING, S. D. & ANDERSON, D. L. 1995. An alternative mechanism of flood basalt formation. *Earth and Planetary Science Letters* **136**, 269–79.

KING, S. D. & ANDERSON, D. L. 1998. Edge-driven convection. *Earth and Planetary Science Letters* **160**, 289–96.

KUSHIRO, I. 1996. Partial melting of a fertile mantle peridotite at high pressure and experimental study using aggregates of diamond. In *Earth processes: reading the isotopic code* (eds A. Basu & S. Hart), pp. 109–22. Geophysical Monograph Series vol. 95

LANGMUIR, C. H., KLEIN, E. M. & PLANK, T. 1992. Petrological systematics of mid-ocean ridge basalts: constraints on melt generation beneath ocean ridges. In *Mantle flow and melt generation at mid-ocean ridges* (eds J. Phipps Morgan, D. K. Blackman & J. M. Sinton), pp. 183–280. American Geophysical Union, Geophysical Monograph no. 71.

LE BAS, M., LE MAITRE, R. W., STRECKEISEN, A. & ZANETTIN, B. 1986. A chemical classification of volcanic rocks based on the total alkali-silica diagram. *Journal of Petrology* **27**, 745–50.

LE PICHON, X. & GAULIER, J. M. 1988. The rotation of Arabia and the Levant Fault system. *Tectonophysics* **153**, 271–94.

LUSTRINO, M. & SHARKOV, E. 2006. Neogene volcanic activity of western Syria and its relationship with Arabian plate kinematics. *Journal of Geodynamics* **42**, 115–39.

MCKENZIE, D. & BICKLE, M. J. 1988. The volume and composition of melt generated by extension of the lithosphere. *Journal of Petrology* **29**, 625–79.

MCKENZIE, D. & O'NIONS, R. K. 1991. Partial melt distributions from inversion of rare earth element concentrations. *Journal of Petrology* **32**, 1021–91.

MTA (MADEN TETKIK VE ARAMA GENEL MÜDÜRLÜĞÜ). 2002. *Diyarbakır sheet of the Geological map of Turkey, 1/500 000 scale*. Ankara: General Directorate of Mineral Research and Exploration.

NICHOLLS, J. 1988. The statistics of Pearce element diagrams and the Chayes closure problem. *Contributions to Mineralogy and Petrology* **99**, 11–24.

PEARCE, J. A. & CANN, J. R. 1973. Tectonic setting of basic volcanic rocks determined using trace element analyses. *Earth and Planetary Science Letters* **19**, 290–300.

PERİNÇEK, D. 1979. *The geology of Hazro-Korudag-Cüngüş-Maden-Ergani-Hazar-Elazig-Malatya Area*. Geological Society of Turkey Special Publication, 34 pp.

POLAT, A., KERRICH, R. & CASEY, J. F. 1997. Geochemistry of Quaternary basalts erupted along the East Anatolian and Dead Sea fault zones of southern Turkey: implications for mantle sources. *Lithos* **40**, 55–68.

RICHARDS, M. A., DUNCAN, R. A. & COURTILLOT, V. E. 1989. Flood basalts and hot-spot tracks: plume heads and tails. *Science* **246**, 103–7.

RICHTER, D. H. & MURATA, K. J. 1966. *Petrography of the lavas of the 1959–60 eruption of Kilauea Volcano, Hawaii*. U.S. Geological Survey Professional Paper 537-D.

ROJAY, B., HEIMANN, A. & TOPRAK, V. 2001. Neotectonic and volcanic characteristics of the Karasu fault zone (Anatolia, Turkey): The transition zone between the Dead Sea transform and the East Anatolian fault zone. *Geodinamica Acta* **14**, 1–3, 197–212.

RUDNICK, R. L. & FOUNTAIN, D. M. 1995. Nature and composition of the continental crust: a lower crustal perspective. *Reviews of Geophysics* **33**, 267–309.

RUKIEH, M., TRIFONOV, V. G., DODONOV, A. E., MININI, H., AMMAR, O., IVANOVA, T. P., ZAZA, T., YSEF, A., AL-SHARA, M. & JOBAILI, Y. 2005. Neotectonic map of Syria and some aspects of Late Cenozoic evolution of the northwestern boundary zone of the Arabian plate. *Journal of Geodynamics* **40**, 235–56.

RUSSELL, J. K. & NICHOLLS, J. 1988. Analysis of petrologic hypotheses with Pearce element ratios. *Contributions to Mineralogy and Petrology* **99**, 25–35.

ŞENGÖR, A. M. C. & KIDD, W. S. F. 1979. Post-collisional tectonics of the Turkish-Iranian plateau and a comparison with Tibet. *Tectonophysics* **55**, 361–76.

SHARKOV, E. V., CHERNYSHEV, I. V., DEVYATKIN, E. V., DODONOV, A. E., IVANENKO, V. V., KARPENKO, M. I., LEBEDEV, V. A., NOVIKOV, V. M., HANNA, S. & KHATIB, K. 1998. New data on the geochronology of upper Cenozoic plateau basalts from the northeastern periphery of the Red Sea rift area (northern Syria). *Doklady Earth Sciences* **358**, 19–22.

SHAW, J. E., BAKER, J. A., MENZIES, M. A., THIRLWALL, M. F. & IBRAHIM, K. M. 2003, Petrogenesis of the largest intraplate volcanic field on the Arabian plate (Jordan): a mixed lithosphere–asthenosphere source activated by lithospheric extension. *Journal of Petrology* **44**, 1657–79.

SOBOLEV, S. V., PETRUNIN, A., GARFUNKEL, Z. & BABEYKO, A. Y. 2005. Thermo-mechanical model of the Dead Sea Transform. *Earth and Planetary Science Letters* **238**, 78–95.

SUN, S. S. & MCDONOUGH, W. F. 1989. Chemical and isotopic systematics of oceanic basalts: implication for mantle composition and processes. In *Magmatism in the Ocean Basins* (eds A. D. Saunders & M. J. Norry), pp. 313–45. Geological Society of London, Special Publication no. 42.

TAKAHASHI, E. & KUSHIRO, A. I. 1983. Melting of a dry peridotite at high-pressures and basalt magma genesis. *American Mineralogist* **68**, 859–79.

TATAR, O., PIPER, J. D. A., GÜRSOY, H., HEIMANN, A. & KOÇBULUT, F. 2004. Neotectonic deformation in the transition zone between the Dead Sea Transform and the East Anatolian Fault Zone, Southern Turkey: a paleomagnetic study of the Karasu Rift Volcanism. *Tectonophysics* **385**, 17–43.

TAYLOR, S. R. & MCLENNAN, S. M. 1985. *The Continental Crust: Its Composition and Evolution*. Blackwell Scientific Publications, 312 pp.

TERLEMEZ, H. C., ŞENTÜRK, K., ATEŞ, S. & ORAL, A. 1997. *Geological map of the Gaziantep-K24 quadrangle, 1:100 000 scale, and accompanying 18 page explanatory booklet*. General Directorate of Mineral Research and Exploration, Ankara.

THIRLWALL, M. F., UPTON, B. G. & JENKINS, C. 1994. Interaction between continental lithosphere and the Iceland plume–Sr–Nd–Pb isotope geochemistry of Tertiary basalts, NE Greenland. *Journal of Petrology* **35**, 839–79.

THORNBER, C. R. & HUEBNER, J. S. 1985. Dissolution of olivine in basaltic liquids: experimental observations and applications. *American Mineralogist* **70**, 935–45.

TOLUN, N. & PAMİR, H. N. 1975. *Explanatory Booklet accompanying the Hatay sheet of the Geological Map of Turkey, 1:500,000 scale*. Ankara: General Directorate of Mineral Research and Exploration, 99 pp.

TURCOTTE, D. L. & EMERMAN, S. H. 1983. Mechanisms of active and passive rifting. *Tectonophysics* **94**, 39–50.

ULU, Ü., ERCAN, T., GENÇ, Ş., METIN, Y., ÇÖREKÇIOĞLU, E., ÖRÇEN, S., KARABIYIKOĞLU, M., GIRAY, S. & YAŞAR, T. 1991. Geology of the Nizip–Yavuzeli–Araban–Belveren district (Gaziantep, SE Anatolia) and petrology and regional distribution of the Cenozoic volcanic rocks. *Bulletin of Geological Congress of Turkey* **6**, 207–27.

WANG, K., PLANK, T., WALKER, J. D. & SMITH, E. I. 2002. A mantle melting profile across the Basin and Range, SW USA. *Journal of Geophysical Research* **107**(B1), 2017, doi:10.1029/2001JB000209, ECV5-1–21.

WEAVER, B. L. & TARNEY, J. 1984. Empirical approach to estimating the composition of the continental crust. *Nature* **310**, 575–7.

WESTAWAY, R. 2003. Kinematics of the middle east and eastern Mediterranean updated. *Turkish Journal of Earth Sciences* **12**, 5–46.

WESTAWAY, R. 2004. Kinematic consistency between the Dead Sea Fault Zone and the Neogene and Quaternary left-lateral faulting in SE Turkey. *Tectonophysics* **391**, 203–37.

WESTAWAY, R., DEMİ, T., SEYREK, A. & LONG, A. 2006. Kinematics of active left-lateral faulting in SE Turkey from offset Pleistocene river gorges: improved constraint on the rate and history of relative motion between the Turkish and Arabian plates. *Journal of the Geological Society, London* **163**, 149–64.

WHITE, R. S. & MCKENZIE, D. 1989. Magmatism at rift zones: the generation of volcanic continental margins and flood basalts. *Journal of Geophysical Research* **94**, 7685–729.

WRIGHT, T. L. 1973. Magma mixing as illustrated by the 1959 eruption, Kilauea volcano, Hawaii. *Geological Society of America Bulletin* **84**, 849–58.

YAZGAN, E., MICHARD, A., WHITECHURCH, H. & MONTIGNY, R. 1983. Le Taurus de Malatya (Turquie Orientale), element de la suture sur-tethysienne. *Bulletin de la Société de Géologique de France* **25**, 59–69.

YILMAZ, Y. 1993. New evidence and model on the evolution of the southeast Anatolian orogen. *Geological Society of America Bulletin* **105**, 251–71.

YURTMEN, S. & WESTAWAY, R. 2001. Neogene to Quaternary volcanism and strike-slip faulting in the Gaziantep Plateau, southeastern Turkey. *Fourth International Turkish Geology Symposium, September 2001 abstract volume*. Çukurova University, Adana, Turkey, pp. 184.

YÜRÜR, T. M. & CHOROWICZ, J. 1998. Recent volcanism, tectonics and plate kinematics near the junction of the African, Arabian and Anatolian plates in the Eastern Mediterranean. *Journal of Volcanology and Geothermal Research* **85**, 1–15.